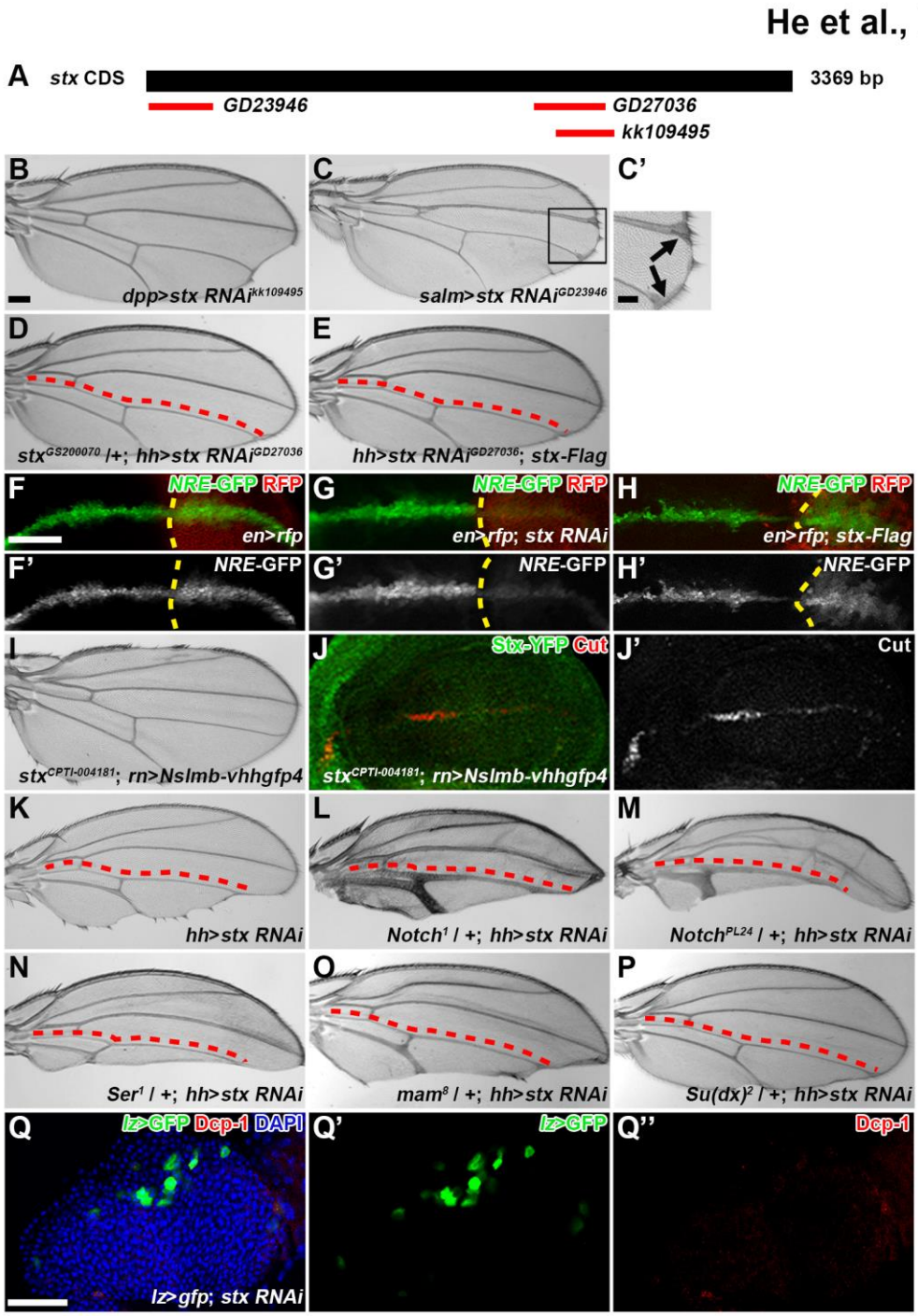

Fig. S1. *stx* positively regulates Notch signaling.

(A) Schematic diagram showing the targeted regions of three *stx* RNAi transgenic lines on the *stx* coding sequence. (B-E) Adult wings of the indicated genotype are shown. Knockdown of *stx* by two additional RNAi lines targeting different coding regions of *stx* resulted in similar wing notching phenotypes (B and C). The magnified box area in panel C is shown (C'); arrows mark small deltas distal to the L3 and L4 longitudinal veins. Overexpression of *stx* using a GS line (D) or a UAS-*stx*-*Flag* transgene (E) largely rescued the notched wing phenotype associated with *stx* RNAi.

(F-H') *NRE*-GFP reporter expression in wing discs of the indicated genotype is shown. Reducing *stx* expression by RNAi decreased *NRE*-GFP expression (G'; cf. F'), while overexpression of *stx* increased *NRE*-GFP activity (H'; cf. F').
(I-J') Adult wing and expression of Stx-YFP and Cut in wing discs of the indicated genotype are shown. Knockdown of *stx* by the deGradFP strategy in a CPTI line, in which a YFP protein trap cassette was inserted into the *stx* locus, resulted in a notched adult wing phenotype (I) and downregulation of Cut expression (J') in the wing disc.
(K-P) Adult wings of the indicated genotype are shown. When one copy of *Notch* (L, M), *Ser* (N) or *mam* (O) was mutated, the loss of wing margin tissue caused by *stx* RNAi (K) was exacerbated. In contrast, this phenotype was partially rescued in *Su(dx)*^{1} heterozygotes (P).
(Q-Q'') The expression of *lz*>GFP and cleaved Dcp-1 in the lymph gland of the indicated genotype is shown. Knocking down *stx* did not induce the cleavage of Dcp-1 in GFP-marked crystal cells.
The adult wings in are shown proximal to the left, with anterior/posterior (a/p) boundaries marked with red dashed lines. The wing discs are shown anterior to the left and ventral at the top, with a/p boundaries marked with yellow dashed lines.
Scale bar, B-E, I and K-P, 100 μm; C', F-H', J, J' and Q-Q'', 50 μm.

He et al., Figure S2

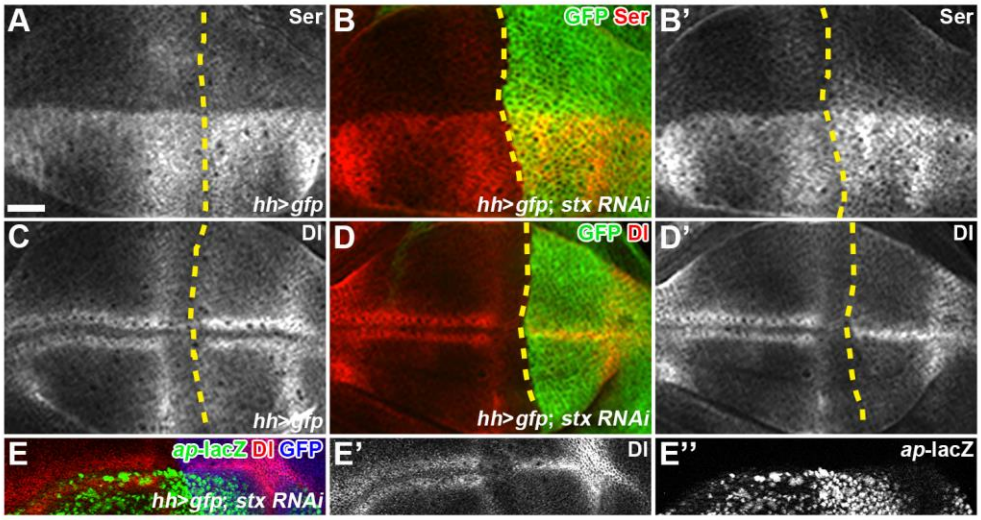

Fig. S2. *stx* does not regulate Dl or Ser expression.

Ser (A-B'), Dl (C-E'), and *ap*-lacZ expression (E, E') in the wing disc of the indicated genotype are shown. In GFP-marked posterior compartment cells where *stx* expression was knocked down by *hh*-Gal4-driven RNAi, Ser protein expression was unaffected (B'; cf. A), but the expression pattern of Dl changed from two stripes (C) to one stripe along the dorsal/ventral (D/V) boundary (D' and E-E''). The dorsal compartment of the wing disc was marked with *ap*-lacZ (E'').

The wing discs are shown anterior to the left and ventral at the top, with a/p boundaries marked with yellow dashed lines.

Scale bar, 50 μm.

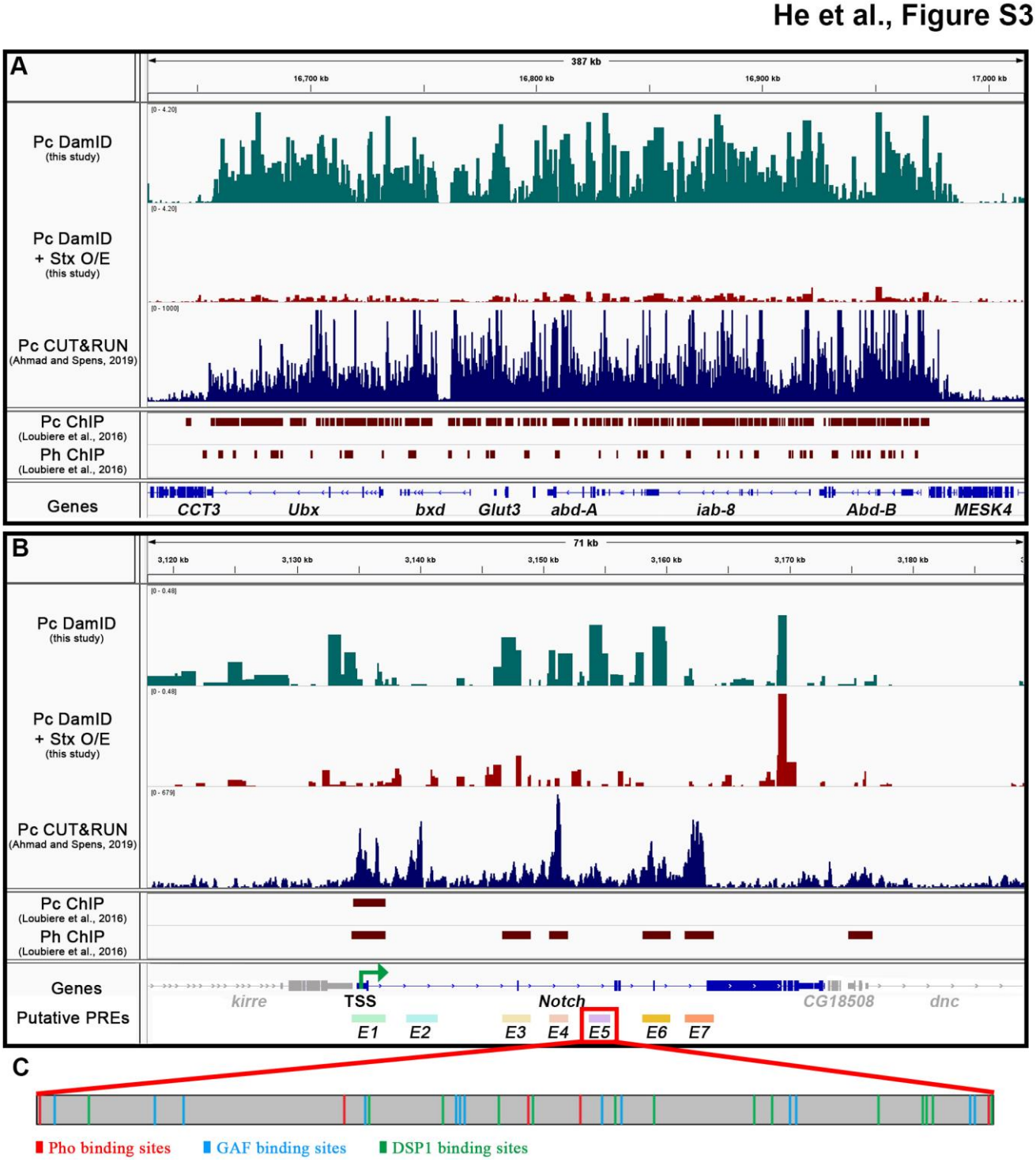

Fig. S3. Pc and Ph recruitment in canonical PcG target genes and the *Notch* locus.

(A) Pc and Ph recruitment to the indicated region containing canonical PcG target genes were compared by analysing three datasets: CUT&RUN and ChIP-seq data from the wing disc in previous studies (Loubiere et al., 2016; Ahmad and Spens, 2019) and the DamID-seq data generated in this study.

(B) Pc and Ph recruitment at the *Notch* locus were compared by analysing three datasets, as shown in A. The putative PREs are displayed as color-coded rectangles that match the PRE GFP reporter activity shown in Figure 4L, M and Figure S4L-N.

(C) Shown are the putative binding sites of Pho, GAGA, and DSP1 in the *E5* region.

He et al., Figure S4

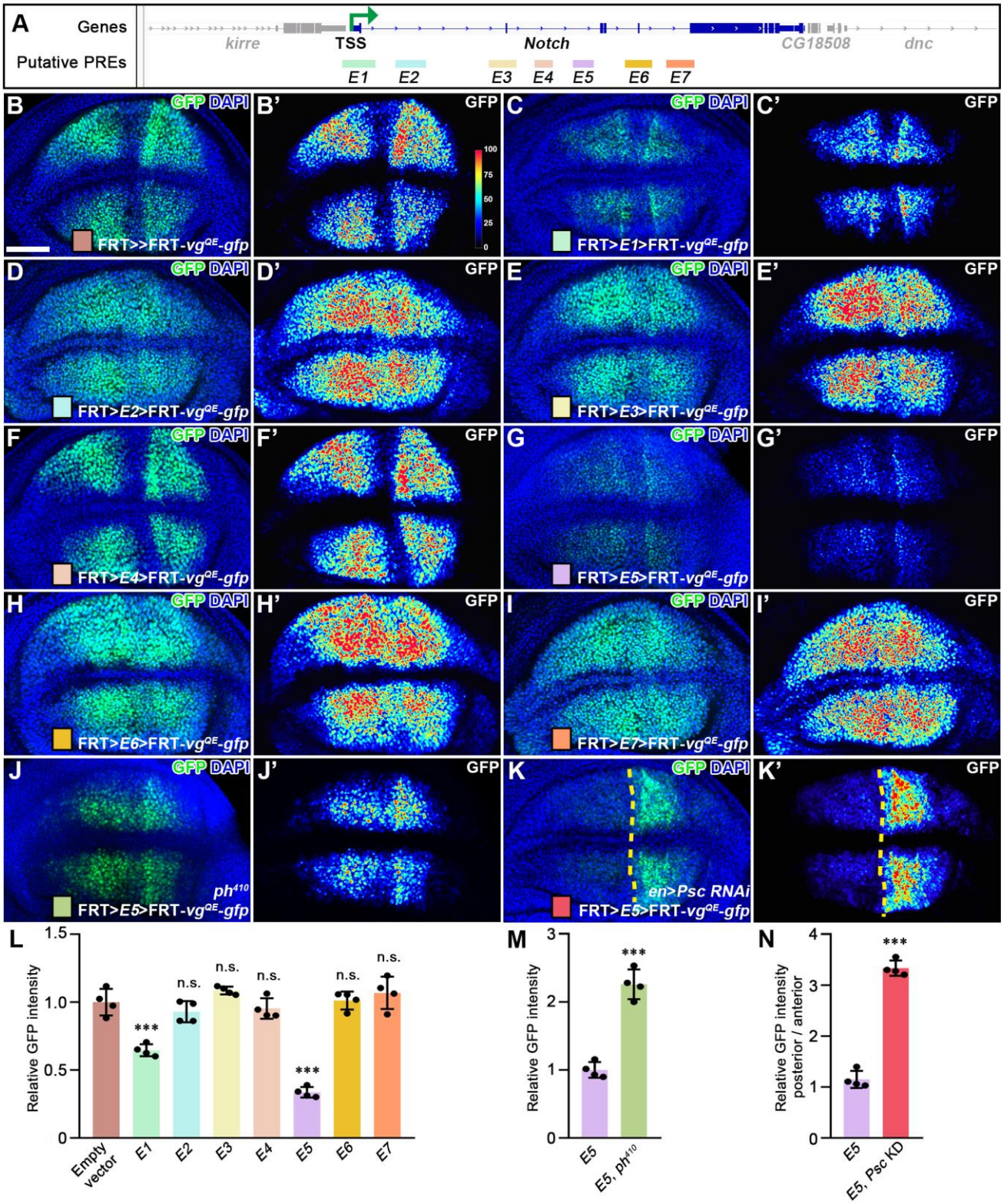

Fig. S4. *E1* and *E5* are potential functional PREs.

(A) Schematic diagram of the putative PREs (rectangles) in the *Notch* locus where each putative PRE is assigned a unique color key that matches the PRE GFP reporter activity shown in panels L-N.

(B-N) GFP reporter expression (B-K) and corresponding heatmap images (B'-K') of relative GFP intensity in wing discs of the indicated genotype are shown. The vertical color bar on the right (B') represents the intensity range. Both *E1* (C') and *E5* (G') were able to repress the expression of GFP reporter, with E5 showing a stronger effect, while the other five fragments had no inhibitory effects on GFP reporter expression (D', E', F', H', I'). Moreover, GFP expression of the *E5* reporter was significantly increased in loss-of-function ph^{410} mutant wing disc (J'; cf. G') and in the posterior compartment of the wing disc where *Psc* was knocked down by *en*-Gal4-driven RNAi (K'; cf. G'). Statistical analyses of relative GFP fluorescence intensity in wing discs of the indicated genotype (n=4) are shown (L-N). GFP activity controlled only by vg^{QE} was used as a normalized standard. Data were presented as mean±S.D, *** $p<0.001$, n.s. $p>0.05$ (One-way ANOVA, Dunnett's multiple comparison tests).

The wing discs are shown anterior to the left and ventral at the top, with a/p boundaries marked with yellow dashed lines.

Scale bar, 50 μm.

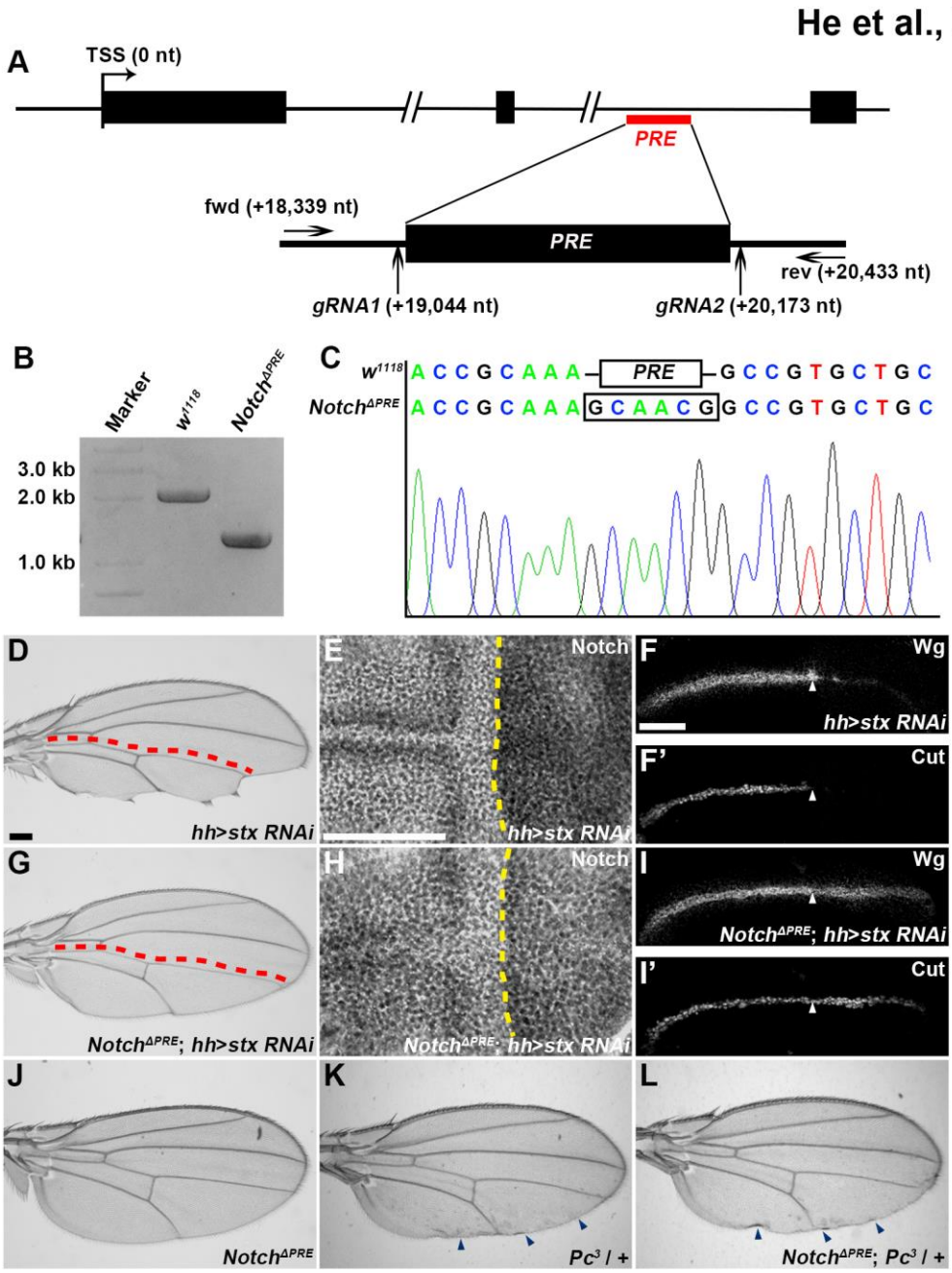

Fig. S5. The expression of Notch in *Notch*$^{\Delta PRE}$ mutant flies is no longer modulated by Stx and Pc.

(A) Schematic diagram showing the location of gRNAs and primers used to generate and validate the *Notch*$^{\Delta PRE}$ allele. (B) Using the forward and reverse primers shown in panel A, PCR products amplified using genomic DNA extracted from w^{1118} and *Notch*$^{\Delta PRE}$ flies, respectively, showed that the 1.1 Kb PRE sequence was removed from the *Notch* locus. (C) A comparison of the Sanger sequencing results of the two PCR products in panel B confirmed that the PRE sequence was deleted *in situ* from the *Notch*$^{\Delta PRE}$ allele.

(D-I') Adult wings (D, G) and the expression of Notch (E, H) and Notch signaling target genes Wg (F, I) and Cut (F', I') in the wing disc of the indicated genotype are shown. Knockdown of *stx* resulted in a notched adult wing phenotype (D) and downregulation of Notch (E), Wg (F), and Cut expression (F') in the wing disc. These phenotypes were largely restored in the $Notch^{\Delta PRE}$ mutant wing blade (G; cf. D) and wing discs (H-I'; cf. E-F'). The arrowhead marks the a/p boundary of the wing disc (F, F', I, I').

(J-L) Adult wings of the indicated genotype are shown. No apparent wing vein phenotype associated with gain-of-function Notch signaling was observed in adult $Notch^{\Delta PRE}$ wings (J), nor did Pc^{3} heterozygosity change this phenotype (L). Note that the posterior wing margin curvature phenotype of the Pc^{3} heterzygous wing (arrowheads in K and L) is due to partial transformation of the methothoracic wing to the metathoracic haltere (Bi et al., 2022), which is not related to Notch signaling alteration.

The adult wings are shown proximal to the left, with a/p boundaries marked with red dashed lines. The wing discs are shown anterior to the left and ventral at the top, with a/p boundaries marked with yellow dashed lines.

Scale bar, D, G and J-L, 100 μm; E-F' and H-I', 50 μm.

He et al., Figure S6

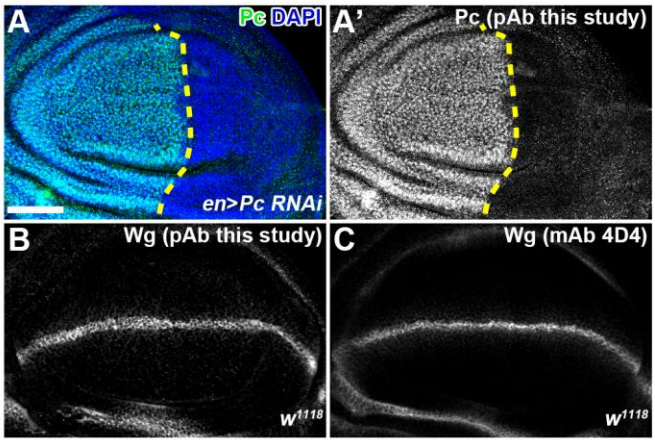

Fig. S6. Validation of the Pc and Wg antibodies generated in this study.

Pc (A, A') and Wg expression (B, C) in the wing disc of the indicated genotype were detected by the indicated antibodies. In posterior compartment cells where *Pc* expression was knocked down by *en*-Gal4-driven RNAi, the expression of Pc protein detected by the rabbit anti-Pc antibody generated in this study was significantly reduced (A'). Rabbit anti-Wg antibody (B) generated in this study and mouse anti-Wg antibody (C) purchased from DSHB (clone 4D4) detected similar Wg expression patterns in the wing pouch.

Wing discs are shown with anterior to the left and ventral at the top, with a/p boundaries marked with yellow dashed lines.

Scale bar, 50 μm.

Table S1. Genetic crosses for figures and supplemental figures

Click here to download Table S1

Table S2. List of primers used in this study

Click here to download Table S2